NATIONAL UNIVERSITZ OF SCIENCE AND TECHNOLOGY
POLITEHNICA BUCHAREST

FACULTATY OF MATERIALS SCIENCE AND TECHNOLOGY

Autor: Eng. Alin Mihai DEMIAN

PhD THESIS- ABSTRACT

RESEARCH ON THE BEHAVIOR OF ALUMINUM ALLOY TYPE 6082 UNDER CAVITATION EROSION IN CORRELATION WITH DIFFERENT STRUCTURAL STATES

Scientific coordinators:
Prof. habil. dr. eng. Brânduşa GHIBAN
Prof.dr.eng. Ilare BORDEAŞU

București 2025

CHAPTER 1 – PHYSICAL METALLURGY OF 6XXX SERIES ALUMINUM ALLOYS

The literature research carried out in this work has shown that, in order to improve the mechanical properties of 6xxx series aluminum alloys, it is essential to understand and apply the correct processing steps, as well as the underlying mechanisms responsible for their strengthening. This literature synthesis clearly indicates that proper homogenization is a critical step prior to the processing of 6xxx series aluminum alloys. Homogenization improves the quality of as-cast precipitates by decomposing and transforming the acicular β-Al_5FeSi phase into the more spheroidal α-Al_8Fe_2Si form and by dissolving hard Mg_2Si particles into the aluminum matrix. Subsequently, the alloy is processed and strengthened through the precipitation of a large number of fine, dispersed Guinier–Preston (GP) zones and β″-type precipitates.

CHAPTER 2 – MATERIAL, RESEARCH METHODOLOGY, AND EXPERIMENTAL PROGRAM

2.1 Material and Research Methodology

The 6082 aluminum alloy samples were provided by COLOR METALS S.R.L. For experimental investigations, specimens in rolled condition (T651 state) were used, corresponding to a heat treatment consisting of solution treatment at 525 °C for 4 hours followed by water quenching, and subsequent artificial aging at 175 °C for 8 hours. The macroscopic appearance of the experimental specimens is shown in Figure 2.1.



Fig. 2.1 - Macroscopic appearance of the 6082 alloy experimental specimens, with various dimensions for conducting the experimental investigations

Artificial aging heat treatments were applied to the experimental specimens in rolled T651 condition at 190 °C, 160 °C, and 140 °C, each with holding times of 1 hour, 12 hours, and 24 hours, respectively. Additionally, specimens coated with WIG welding were also included in the study.

The heat treatments were performed in a Nabertherm furnace within the Laboratory of Metallic Materials Science and the Physical Metallurgy Section of the University Politehnica of Bucharest. For each type of heat treatment, six tests were conducted to determine the mechanical properties: tensile strength, yield strength, elongation, toughness, hardness, and microhardness. Grain size determination was carried out according to ASTM E3, ASTM E407, and ASTM E112 standards, using Barker's electrolytic reagent at 100× magnification. Structural investigations were conducted using an OLYMPUS optical microscope. The mechanical properties of the heat-treated specimens were evaluated using a Walter + Bai AD universal testing machine, model LFV 300 (Switzerland). Impact resistance was determined by measuring the KCV values using a Walter + Bai Charpy Pendulum impact tester with a capacity of 300 J.

Macroscopic structural analysis was performed with an OLYMPUS SZX stereomicroscope equipped with QuickMicroPhoto 2.2 software, while microscopic analysis was conducted using an OLYMPUS optical microscope with Image Pro Plus software. X-ray diffraction analysis was carried out using a D8 Discover diffractometer (Bruker, Germany) equipped with a Cu anode tube

(λ = 1.540598 Å) and a 1D Lynx Eye detector. The diffraction patterns were recorded with an angular increment of 0.040°, a scanning speed of 1 s/step, and a measurement range of 2θ = 10°–100°.

Scanning electron microscopy (SEM) analysis was performed using a Thermo Fisher Quattro S scanning electron microscope. Cavitation erosion behavior and resistance tests were conducted at the Politehnica University of Timișoara in the specialized laboratory (see Fig. 2.2). To interpret the results regarding structural response and resistance to cyclic cavitation loading, specific diagrams were constructed, containing all relevant data.

2.2 Experimental Program of This Study

Experimental specimens obtained from Color Metals S.R.L. were used to prepare test samples for the various experiments conducted in this study. The specimens with a thickness of 30 mm, in T651 delivery condition, were subjected to different artificial aging heat treatments at 190 °C, 160 °C, and 140 °C, each for three holding durations: 1 hour, 12 hours, and 24 hours. All specimens were structurally, physically, and mechanically evaluated, followed by cavitation erosion tests to assess the behavior of this class of metallic material under cavitation erosion conditions.

Finally, a structural correlation was established between mechanical behavior, microstructural features, cavitation erosion resistance, and fractographic appearance. The study concludes with original contributions and future perspectives for experimental research. The experimental program that supports the achievement of the main proposed objectives is illustrated in Fig. 2.3.

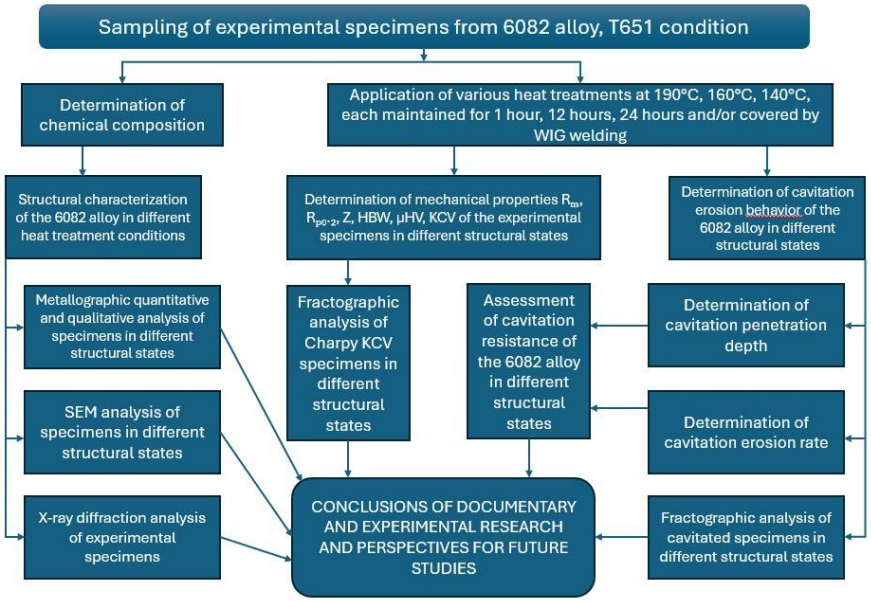


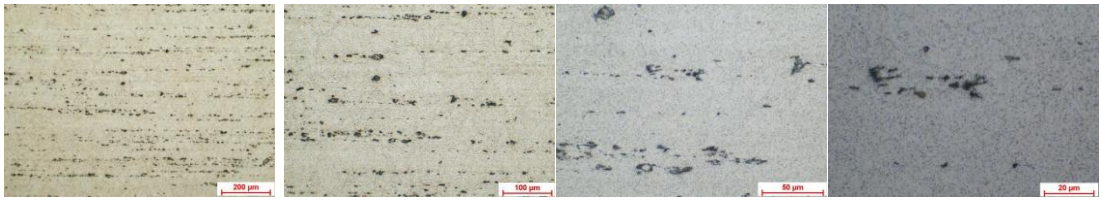
Fig. 2.2 - Experimental Program of This Research

CHAPTER 3 – STRUCTURAL CHARACTERIZATION OF 6082 ALUMINUM ALLOY IN DIFFERENT HEAT TREATMENT CONDITIONS

3.1 Analysis Using Optical Metallographic Microscopy

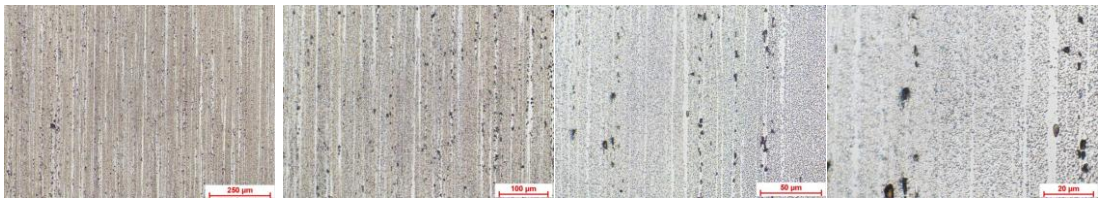
The structural analysis performed using optical metallographic microscopy is of great importance, providing essential information for the structural characterization of a metallic material. The results of the metallographic analysis of 6082 aluminum alloy, subjected to different artificial aging heat treatment conditions, are presented in Figures 3.1 to 3.10 and are compared with the untreated sample.

The microstructural analysis of the alloy in the as-delivered T651 condition is shown in Figure 3.1. After etching with 5% hydrofluoric acid, the solid solution and the presence of fine Mg_2Si particles and α-AlFeSi platelets aligned along the plastic deformation direction can be observed. At high magnification, the maximum size of the Mg_2Si particles is between 1–3 µm, while the α-AlFeSi platelets appear very fine, under 1 µm. Following the application of artificial aging treatments, a more abundant precipitation of Mg_2Si particles and α-AlFeSi platelets is observed. Additionally, as the aging duration increases at each treatment temperature, there is a notable growth in particle size, particularly for the Mg_2Si phase (see Figures 3.2 to 3.10).



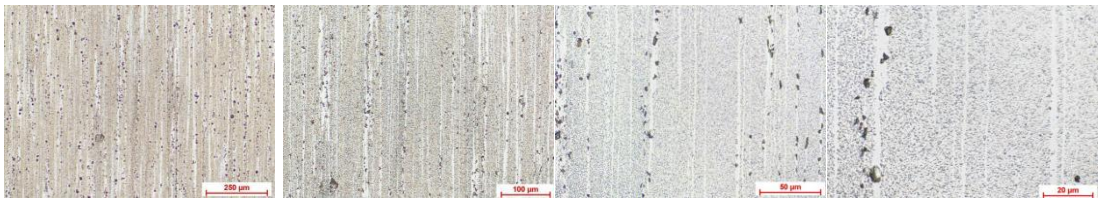
a b c d

Fig. 3.3 - Microstructural appearance of the 6082 alloy in T651 condition – reference sample (without artificial aging heat treatment), at various magnifications under the microscope:
a - x100; b - x200; c - x500; d - x1000



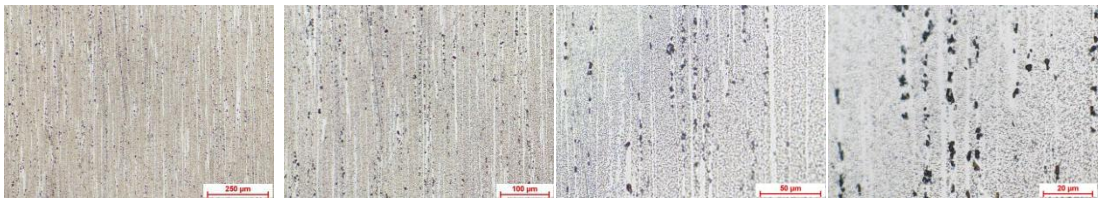
a b c d

Fig. 3.4 - Microstructural appearance of the 6082 alloy in T651 condition + artificial aging heat treatment at 190 °C/1h, at various microscope magnifications:
a - x100; b - x200; c - x500; d - x1000



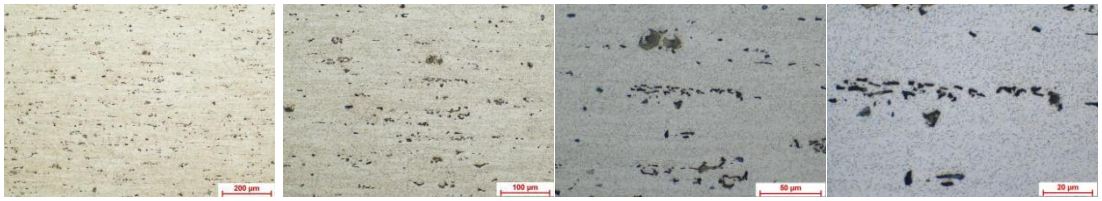
a b c d

Fig. 3.5 - Microstructural appearance of the 6082 alloy in T651 condition + artificial aging heat treatment at 190 °C/12h, at various microscope magnifications:
a - x100; b - x200; c - x500; d - x1000



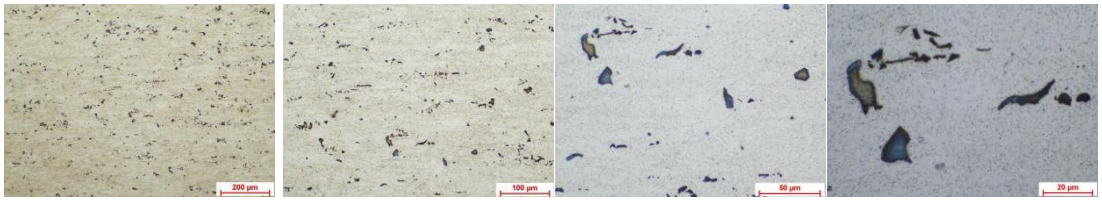
a b c d

Fig. 3.6 - Microstructural appearance of the 6082 alloy in T651 condition + artificial aging heat treatment at 190 °C/24h, at various microscope magnifications:
a - x100; b - x200; c - x500; d - x1000



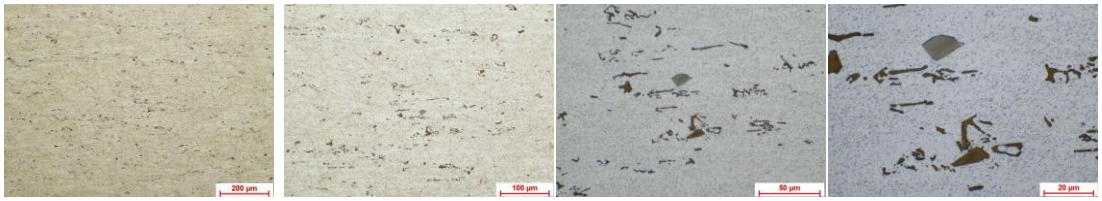
a b c d

Fig. 3.7 - Microstructural appearance of the 6082 alloy in T651 condition + artificial aging heat treatment at 160 °C/1h, at various microscope magnifications:
a - x100; b - x200; c - x500; d - x1000



a b c d

Fig. 3.8 - Microstructural appearance of the 6082 alloy in T651 condition + artificial aging heat treatment at 160 °C/12h, at various microscope magnifications:
a - x100; b - x200; c - x500; d - x1000



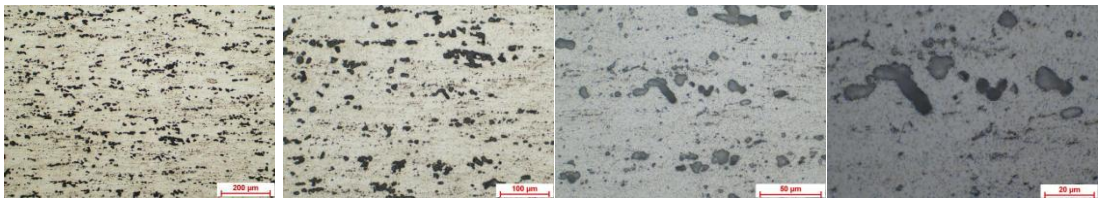
a b c d

Fig. 3.9 - Microstructural appearance of the 6082 alloy in T651 condition + artificial aging heat treatment at 160 °C/24h, at various microscope magnifications:
a - x100; b - x200; c - x500; d - x1000



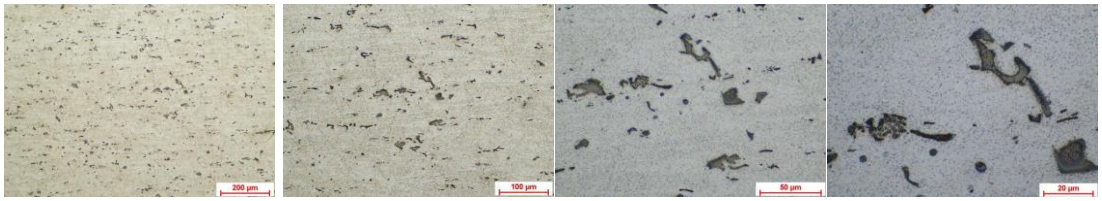
a b c d

Fig. 3.10 - Microstructural appearance of the 6082 alloy in T651 condition + artificial aging heat treatment at 140 °C/1h, at various microscope magnifications:
a - x100; b - x200; c - x500; d - x1000



a b c d

Fig. 3.11 - Microstructural appearance of the 6082 alloy in T651 condition + artificial aging heat treatment at 140 °C/12h, at various microscope magnifications:
a - x100; b - x200; c - x500; d - x1000

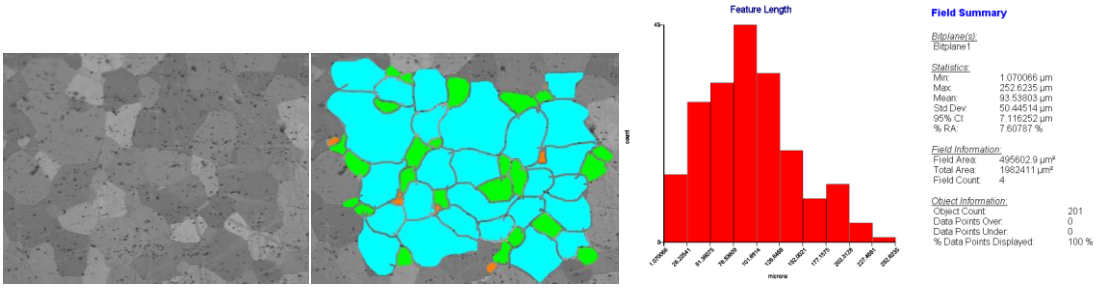


a b c d

Fig. 3.12 - Microstructural appearance of the 6082 alloy in T651 condition + artificial aging heat treatment at 140 °C/24h, at various microscope magnifications:
a - x100; b - x200; c - x500; d - x1000

3.2 Grain Size Determination of 6082 Alloy in Different Structural Conditions

The results regarding the grain size determination of the experimental specimens after applying various artificial aging heat treatments are presented based on quantitative metallographic analysis performed in accordance with ASTM E3, ASTM E407, PO-043, PO-042, and PO-044, using Barker's reagent and examined at 100× magnification, as shown in Figure 3.11 for the reference specimen. The analysis of the grain size values leads to the following observations: the largest grain size was recorded for the untreated reference specimen, with an average grain size of 94 µm, corresponding to ASTM E112 grain size number 4. For the specimens heat treated at 190 °C with various holding durations, the grain size ranged between 63–68 µm, corresponding to grain size number 5 according to ASTM E112. For those heat treated at 160 °C, the grain size ranged between 56–59 µm, corresponding to grain size number 5.5. Finally, the specimens aged at 140 °C showed grain sizes between 48–53 µm, corresponding to ASTM E112 grain size number 5.5–6.



a b c

Fig. 3.13 - Grain Size Determination of 6082 Alloy, T651 Condition, Reference Sample:
a – captured image; b – analyzed image; c – statistical analysis

The analysis of the results from the grain size value histogram of the 6082 aluminum alloy specimens in different structural states (Figure 3.21) leads to the following observations:
The application of artificial aging heat treatments results in a reduction of grain size, regardless of the applied temperature or holding time. Specifically, grain size decreases from class 4 (for the reference, untreated specimen) to classes 5 or even 5.5, according to ASTM E112, in the heat-treated specimens. The smallest grain sizes were recorded in the specimens aged at 140 °C, characterized by fine grains corresponding to class 5.5 (ASTM E112), compared to the class 4 grains observed in the as-delivered T651 condition of the untreated sample.

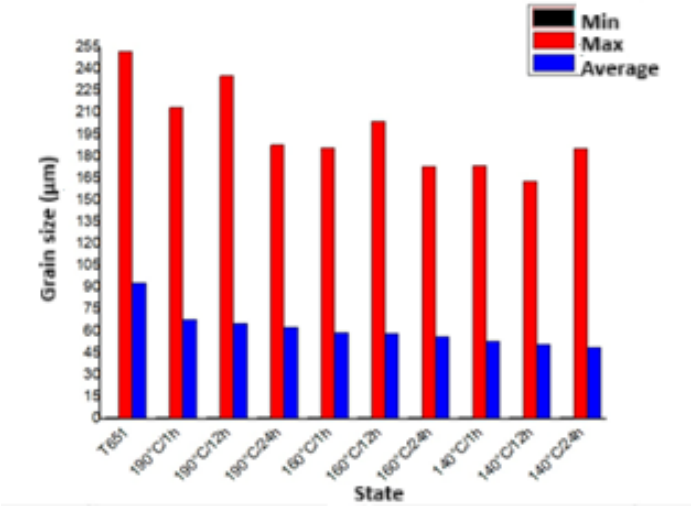


Fig. 3.14 - Histogram of Grain Size Values for 6082 Alloy in Different Structural Conditions

3.3 X-ray Diffraction Analysis

The diffractometric analysis for phase identification in the experimental alloy in T651 condition, subsequently subjected to various aging treatments, is presented in Figure 3.22

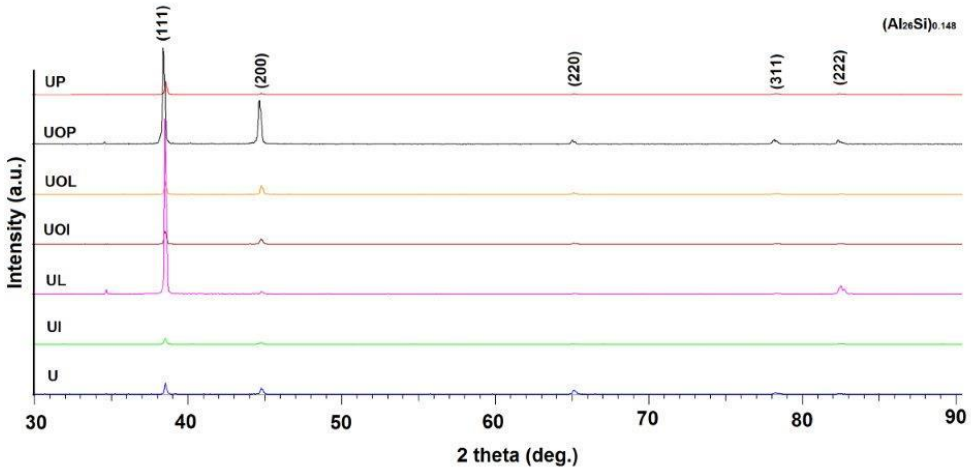
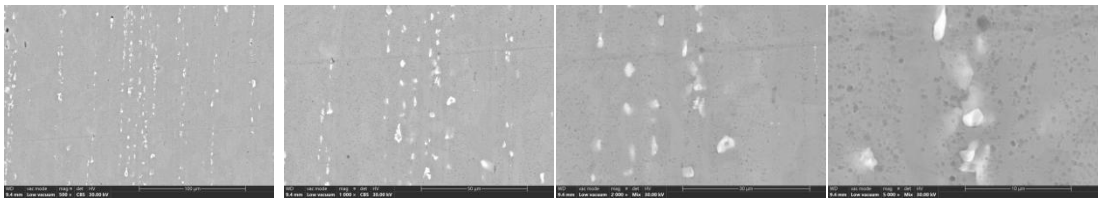


Fig. 3.15 - Diffractometric Analysis of the Experimental Alloy in Rolled T651 Condition and Subsequently Subjected to Various Aging Treatments

Qualitative phase analysis by X-ray diffraction revealed the polycrystalline nature of the analyzed samples. The crystallographic phases were identified using the ICDD Release 2015 database. The unit cell parameters and crystallite size were calculated using the Rietveld refinement method with the TOPAS software and the FindIt database, corresponding to the PDF card: $Al_{0.97}Mn_{0.03}$ (01-074-5245), as shown in Table 3.2. A detailed phase analysis of the experimental alloy indicates that the α solid solution metallic matrix has a lattice parameter of 74.5 nm. The Mg_2Si and α-AlFeSi phases could not be identified due to their very low presence. However, it is worth noting that the lattice parameter changes significantly with the application of different aging treatments, ranging from 55.5 nm to 75.5 nm.

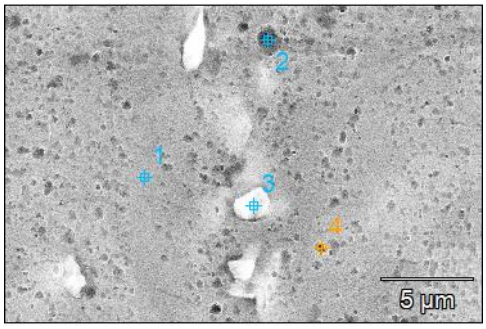
3.4 Scanning Electron Microscopy (SEM) Analysis

The scanning electron microscopy (SEM) analysis was performed on the specimens with the longest holding time at each aging temperature, namely 190 °C, 160 °C, and 140 °C. The analysis focused on both the compositional identification of the strengthening phases within the metallic matrix and the distribution of alloying elements. It is observed that the SEM images are generally similar, with differences arising mainly from particle size and slight variations in local chemical composition. In the case of the 6082 alloy aged at 190 °C for 24 hours, geometrically shaped Mg_2Si particles, plate-like α-AlFeSi particles, and globular complex particles of the type ($Mg_xMn_\gamma Fe_zSi_t$) are visible (**Figure 3.23**). The distributions of magnesium and aluminum are homogeneous, and the images shown in **Figures 3.24 i, j, and k** confirm the presence of these complex particles. The maximum particle size is approximately 5 μm, as illustrated in both **Figure 3.23 d** and Figure 3.24 a.

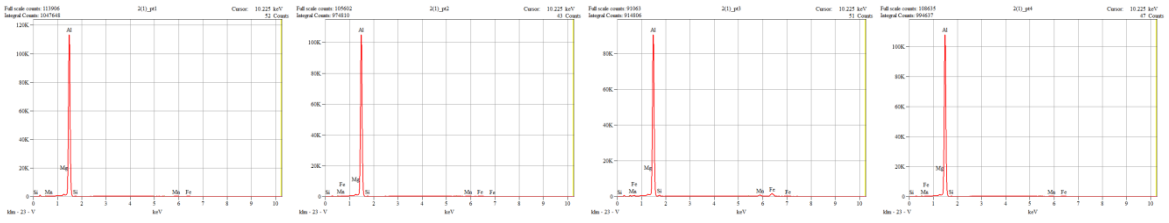


a **b** **c** **d**

***F*ig.3.16 - SEM Images of the Experimental 6082 Aluminum Alloy, T651 Condition, Aged at 190 °C/24h, Etched with 5% Hydrofluoric Acid, at Various Microscope Magnifications: a - x500; b - x1000; c - x2000; d - x5000**



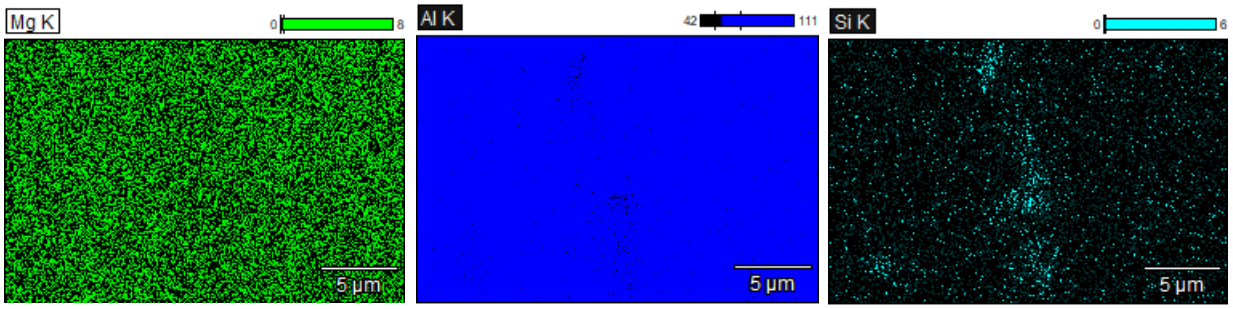
a



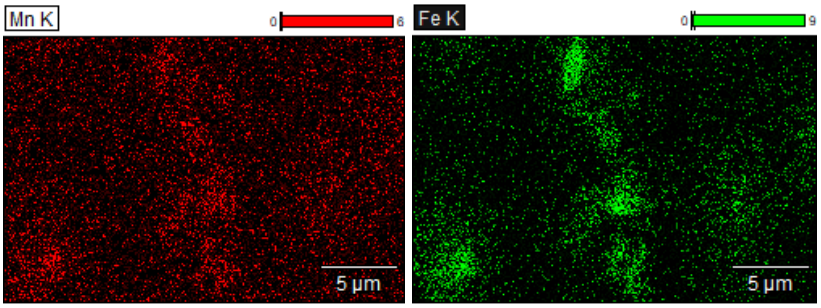
b c d e

zona	*Micro-compoziție locală (%gr.)*				
	Mg	*Al*	*Si*	*Mn*	*Fe*
1	0.59	98.81	0.00	0.37	0.24
2	0.60	98.36	0.00	0.52	0.52
3	0.52	88.73	2.12	2.34	6.28
4	0.57	98.51	0.00	0.53	0.39

f



g h i



j k

Fig. 3.17 - Quantitative and Qualitative SEM Analysis of the Experimental 6082 Aluminum Alloy, T651 Condition, Aged at 190 °C/24h, Etched with 5% Hydrofluoric Acid: a – SEM image with indicated investigation points; b,c,d,e- EDAX of the investigated points; f – local microcomposition of the investigated points; g – magnesium distribution; h – aluminum distribution; i – silicon distribution; j – manganese distribution; k – iron distribution

CHAPTER 4 – MECHANICAL BEHAVIOR OF 6082 ALUMINUM ALLOY IN DIFFERENT STRUCTURAL CONDITIONS

4.1 Determination of the Mechanical Properties of the Experimental Alloy in Different Heat Treatment Structural Conditions

A complete characterization of the metallic material was carried out by determining its mechanical properties. Following the application of artificial aging heat treatments, the resulting mechanical property values are summarized in **Figures 4.1 to 4.6.** As a general conclusion, it can be observed that aging treatments at 190 °C, 160 °C, or 140 °C with various holding times (1h, 12h, or 24h) lead to an increase in tensile strength, yield strength, and impact toughness.

The aging treatment at 140 °C for 24 hours resulted in the highest mechanical property values, namely 402 MPa (ultimate tensile strength), 321 MPa (yield strength), and 30 J/cm² (Charpy impact energy – KCV), compared to the untreated reference alloy, which exhibited 208 MPa (ultimate tensile strength), 112 MPa (yield strength), and 25 J/cm² (KCV).

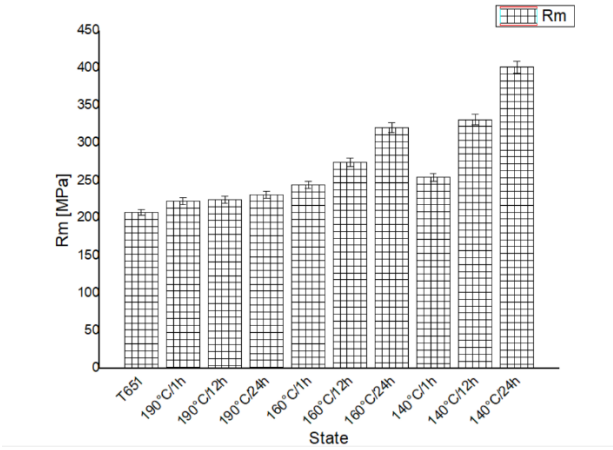


Fig. 4.1 - Histogram of ultimate tensile strength values of the experimental 6082 alloy in different structural conditions

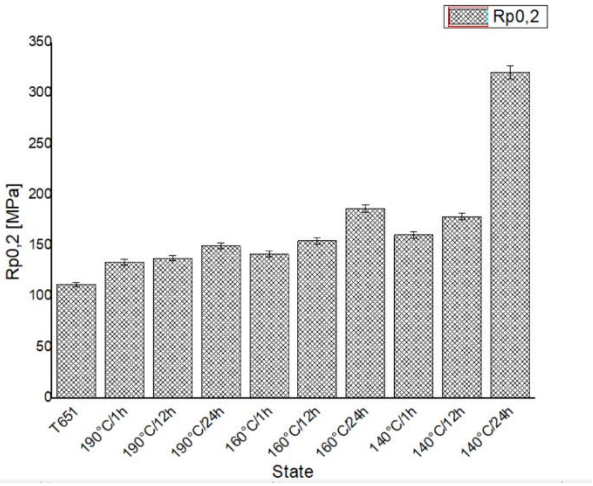


Fig. 4.2 - Histogram of yield strength values of the experimental 6082 alloy in different structural conditions

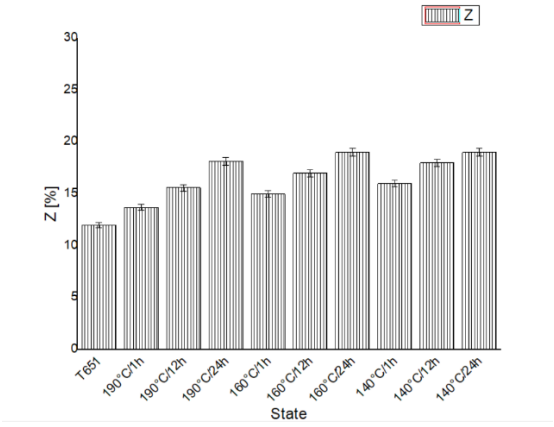


Fig. 4.3 - Histogram of reduction of area values of the experimental 6082 alloy in different structural conditions

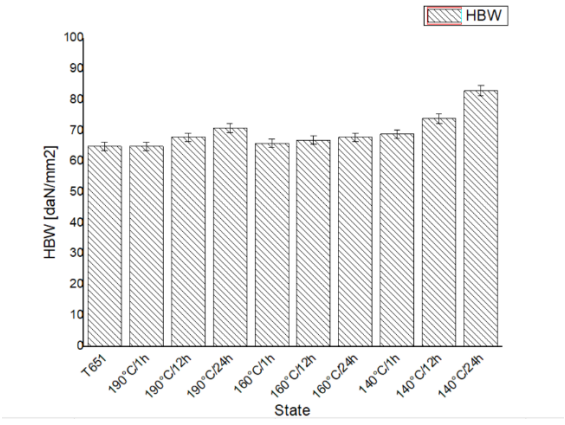


Fig. 4.4 - Histogram of hardness values of the experimental 6082 alloy in different structural conditions

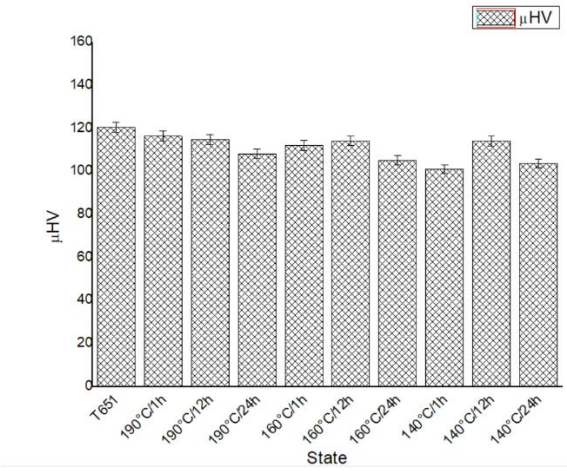


Fig. 4.5 - Histogram of microhardness values of the experimental 6082 alloy in different structural conditions

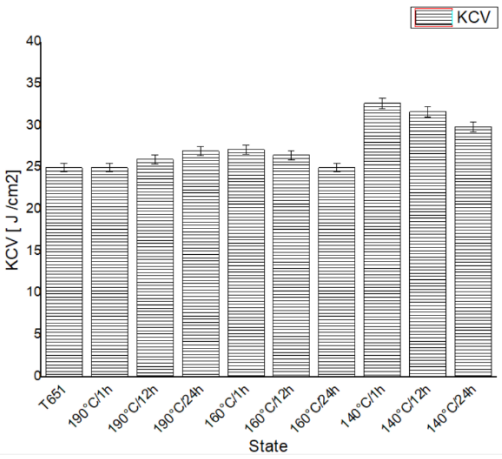


Fig. 4.6 - Histogram of impact toughness values of the experimental 6082 alloy in different structural conditions

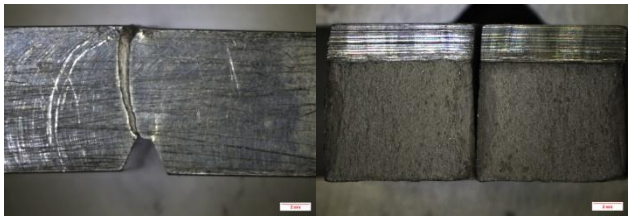
4.2 Stereomacroscopic Fractographic Analysis of the Impact Test Specimens of 6082 Aluminum Alloy

A fractographic study of the fracture surfaces of the Charpy KCV impact test specimens was conducted as a novel element of this research. The fractographic analysis was performed using a stereomicroscope at macroscopic scale, allowing for the identification of the main structural features associated with dynamic impact fracture. Specimens corresponding to 1-hour and 24-hour holding times were examined for each aging heat treatment temperature — 190 °C, 160 °C, and 140 °C — in order to identify structural elements that differentiate the fracture behavior.
As a general observation, the fracture is dynamic, displaying a fibrous appearance, with variations in the propagation of the fracture front due to the different structural states of the specimens.



a b

Fig. 4.7 - Stereomacroscopic appearance of the Charpy V-notch impact specimens made of 6082 aluminum alloy, T651 condition (reference sample, U): a – longitudinal section; b – transverse section



a b

Fig. 4.8 - Stereomacroscopic appearance of the Charpy V-notch impact specimens made of 6082 aluminum alloy, T651 + 190 °c/1h condition (sample UP): a – longitudinal section; b – transverse section



a b

Fig. 4.9 - Stereomacroscopic appearance of the Charpy V-notch impact specimens made of 6082 aluminum alloy, T651 + 190°C/24h (sample UL): a – longitudinal section; b – transverse section



a b

Fig 4.10 - Stereomacroscopic appearance of the Charpy V-notch impact specimens made of 6082 aluminum alloy, T651 + 160°C/1h (sample UI): a – longitudinal section; b – transverse section



a b

Fig. 4.11 - Stereomacroscopic appearance of the Charpy V-notch impact specimens made of 6082 aluminum alloy, T651 + 160°C/24h (sample UOP): a – longitudinal section; b – transverse section



c d

Fig. 4.12 - Stereomacroscopic appearance of the Charpy V-notch impact specimens made of 6082 aluminum alloy, T651 + 140°C/1h (sample UOL): a – longitudinal section; b – transverse section

CHAPTER 5 – CAVITATION BEHAVIOR OF THE EXPERIMENTAL 6082 ALUMINUM ALLOY IN DIFFERENT STRUCTURAL CONDITIONS

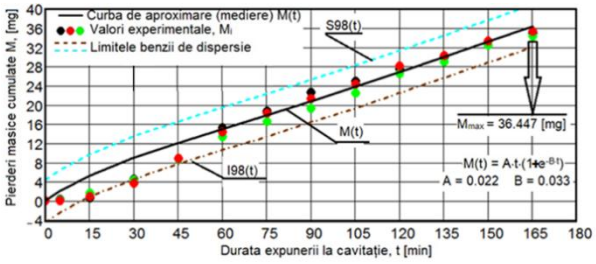
This chapter presents the specific diagrams of cavitation behavior and resistance obtained both for the specimen in the as-delivered T651 condition and for the specimens subjected to various heat treatments — three for each artificial aging temperature: 190 °C, 160 °C, and 140 °C — as well as one specimen with a surface remelted by the WIG method.

5.1 Behavior of the Experimental Alloy in the As-Delivered Condition (Reference – T651)

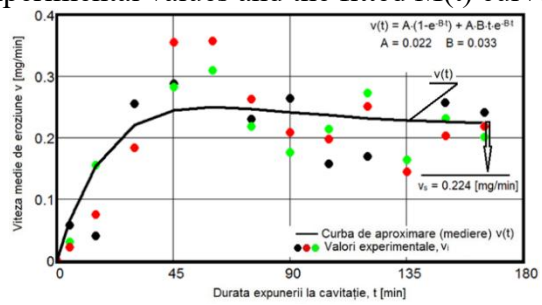
5.1.1 Diagrams and Specific Parameters of Cavitation Erosion Behavior and Resistance of the Experimental Alloy – Reference Sample

The specific diagrams of cavitation behavior and resistance for the experimental specimens of the alloy in the as-delivered condition (reference sample) are presented in **Fig. 5.1**. In accordance with laboratory practice, the legends detail information on experimental values, testing accuracy, and the parameters recommended by ASTM G32-2016 [15] for assessing structural behavior and resistance under cyclic loading by micro-jets and shock waves. **Figure 5.1** incorporates the results obtained from the three specimens tested in the rolled semifinished state (reference condition). The experimental values of the three specimens in **Fig. 5.1** are represented by red, green, and black points, each determined over twelve intermediate periods (one of 5 minutes, one of 10 minutes, and ten intermediate periods of 15 minutes). Based on recent research findings reported in the literature [2-5, 7, 8, 21-29], the following observations can be made:

- The evolution of the mean curve of cumulative mass loss, M(t), shown in **Fig. 5.1a**, is convex during the initial stage of testing (0–45 minutes) and subsequently exhibits linear growth during the final stage (45–165 minutes) up to the maximum value, M_{max}.
- The mean erosion-rate curves, v(t), in **Fig. 5.1b** reach a peak within 30–75 minutes and then decrease asymptotically toward the final stabilization rate, v_s. As demonstrated in the chapters addressing mechanical properties and structural degradation morphology, this evolution reflects the alloy's microstructure and mechanical properties resulting from its heat-treatment regime.
- The mean standard deviation for the reference specimens is $\sigma = 2.213$, corresponding to an approximation error of ± 2 % between the experimental values and the fitted M(t) curve.



a) Variation of mass loss with cavitation duration: mean standard deviation σ = 2.213 (approximation error ± 2%)



b) Variation of erosion rate with cavitation duration

Figură 5.1 - Specific Diagrams of the Experimental Specimens in the As-Delivered Condition, T451–651

5.1.2 Morphology of structural degradation in cavitation-tested specimens – reference sample

The microstructural analysis results for the reference specimens subjected to cavitation are presented in **Fig. 5.2**. The images in **Fig. 5.2** were captured both with a stereomicroscope, at various magnifications, and with an optical metallographic microscope. The comparative results for the maximum cavitation-penetration depth measured with the stereomicroscope and the optical microscope are shown in **Fig. 5.2a** and summarized in **Table 5.1**. The maximum penetration depth in the T651 specimens is essentially identical in the two analyses 490 µm with the stereomicroscope and 491 µm with the optical microscope demonstrating the reproducibility of measurements across different microscopes.

The fractographic assessment performed with the stereomicroscope is illustrated in **Fig. 5.2b** and **5.2c**, which show a frontal view of the cavitation-damaged surface featuring numerous, interconnected pits and a rough cavitated morphology. Quantitative analysis of the diameters of the cavitation-affected areas (summarized in **Table 5.1**) indicates that the total area damaged by cavitation erosion is approximately 85 %, while the most severely affected region accounts for 74 %, as depicted in **Fig. 5.2d, e, and f**.

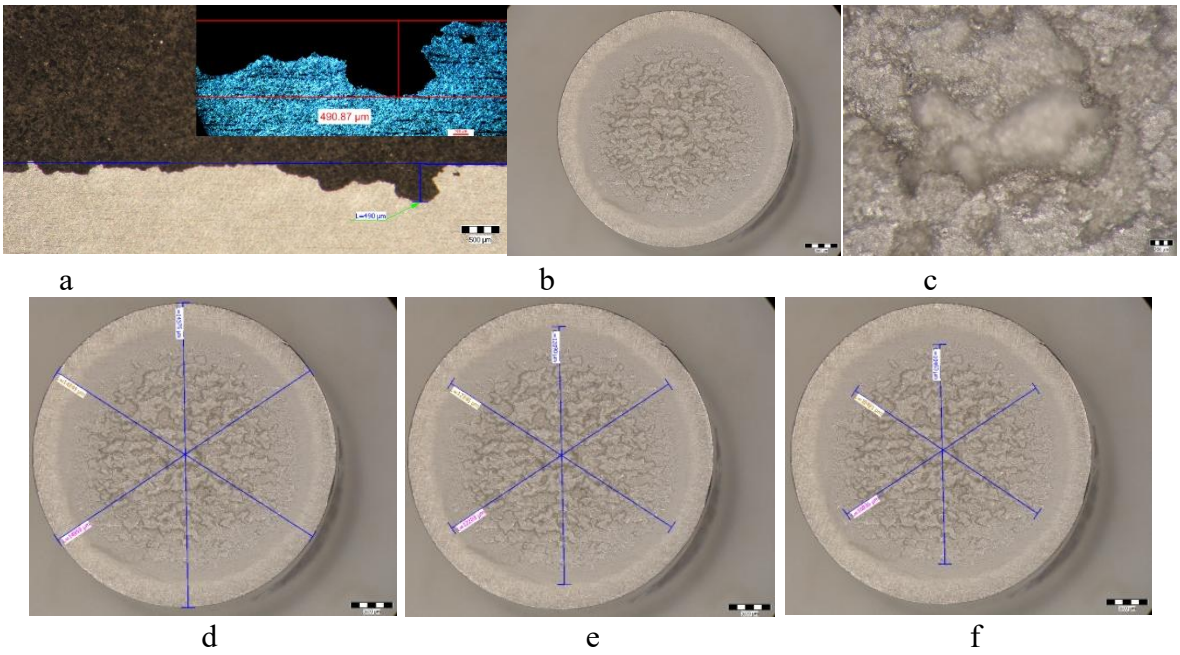


Fig. 5.2 - Quantitative and Qualitative Metallographic Analysis of the Surface of the Experimental 6082 Aluminum Alloy Specimen, As-Delivered Condition – Reference Sample (T651 temper: solution heat-treated at 525 °C for 4 hours, water-quenched): a - images showing the measurement of maximum cavitation penetration depth (background – stereomicroscopic view, top right – image from metallographic microscope); b – frontal section image under stereomicroscope, x8 magnification; c – detail from image b, x56 magnification; d – stereomicroscopic image showing diameter measurements of the cavitation-tested specimen; e – stereomicroscopic image showing diameter measurements of the entire cavitation-affected area; f – stereomicroscopic image showing diameter measurements of the most severely cavitated zone.

5.5 Evaluation of Cavitation Resistance of 6082 Alloy Experimental Specimens in Different Structural Conditions

The histograms in **Fig. 5.23** and **Fig. 5.24** illustrate the differences in resistance to hydrodynamic loading caused by vibratory cavitation observed across the 11 investigated conditions. The notation used is simplified: by temperature and holding time, or by WIG for the remelting regime. The histogram in **Fig. 5.23** allows for an evaluation of the cavitation resistance of the specimen surface structures. The ratio between the values of the R_{cav} parameter provides insight into the differences in cavitation resistance among the surface structures and offers information on the effects of the applied heat treatment regimes as well as the WIG remelting process.

Furthermore, the data from the histogram shown in **Fig. 5.24** reveal the relationship between average erosion depth and the structural resistance to cavitation erosion. Specifically, the greater the cavitation resistance, the smaller the eroded surface area and the dimensions of the formed cavities.

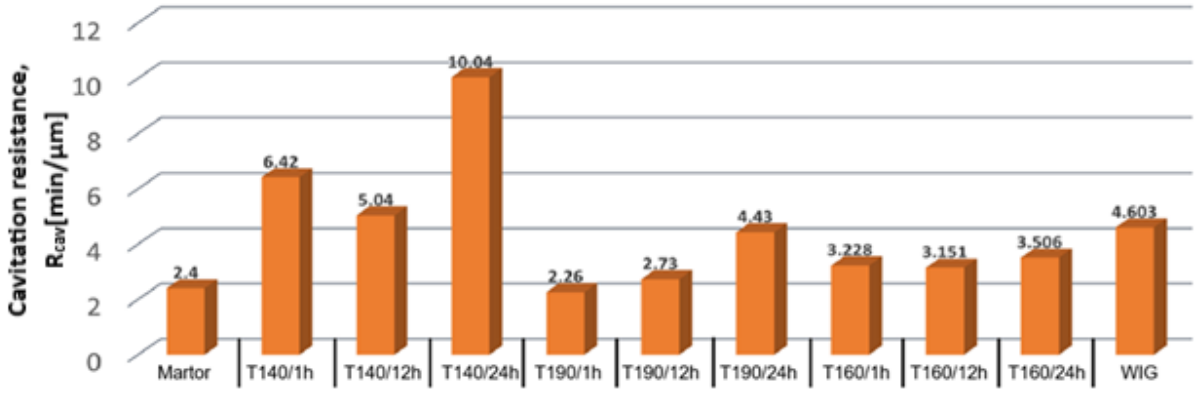


Fig. 5.3 - Histogram comparing the cavitation resistance of 6082 alloy in different structural conditions

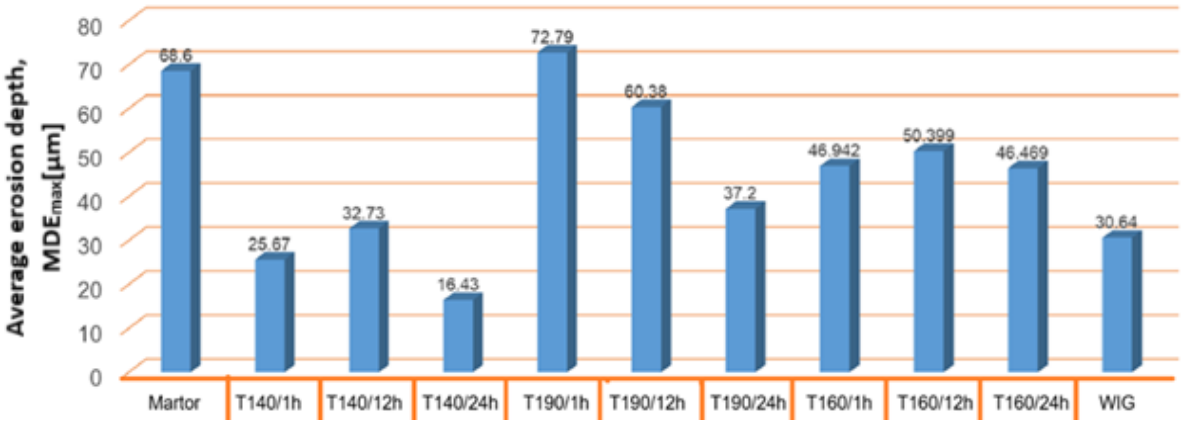


Fig. 5.4 - Histogram comparing the erosion depths of 6082 alloy in different structural conditions

When compared to the as-received condition (semifinished state), using either of the two parameters (R_{cav} or MDE_{max}), it becomes evident that the structure with the highest cavitation resistance the one showing the smallest cavity size after 165 minutes of cavitation exposure is that of the specimens treated at 140°C for 24 hours. Conversely, the weakest resistance, with the largest erosion area and cavity dimensions, is observed in the specimens treated at 190°C for 1 hour.

The improvement in cavitation erosion resistance brought by the applied heat treatment regimes or WIG remelting, relative to the as-received condition (reference sample), expressed through either parameter, is as follows: 2.67 times for T140°C/1h, 2.1 times for T140°C/12h, 4.18 times for T140°C/24h, 13.75% for T190°C/12h, 84.6% for T190°C/24h, 34.5% for T160°C/1h, 31.3% for T160°C/12h, 46.1% for T160°C/24h, and 91.8% for the WIG condition.

The increase in resistance provided by the T140°C/24h treatment is 2.27 times greater than that of the T160°C/24h condition, 2.86 times greater than the T190°C/24h condition, and 2.18 times greater than the WIG-treated structure. Comparing the resistance obtained through WIG remelting with the T160°C/24h and T190°C/24h treatments reveals improvements ranging from 4% to approximately 31%, indicating that WIG remelting may be suitable for components operating under moderate cavitation conditions.

However, the T190°C/1h treatment results in an insignificant decrease in resistance around 0.6% compared to the semifinished structure, suggesting that this regime is not suitable for the heat treatment of components exposed to cavitation, regardless of its intensity. On the other hand, the other regimes, especially those at 140°C, are recommended for components such as pump rotors and boat propellers operating under severe hydrodynamic cavitation conditions.

Based on the analysis of the results presented in this chapter, the following conclusions can be drawn:

- the differences between the experimental values and their dispersion relative to the fitted curves M(t) and v(t), expressed through the tolerance field and standard deviation, indicate that the semifinished material from which the specimens were made exhibits a microstructure characterized by large grain size and intermetallic compounds, which results in a wide variation of the mechanical properties (R_m, $R_{p0.2}$, HB, A_5, and KCU – see Table 4.1);

- the behavior of the M(t) curve concave or convex in the initial stage of cavitation exposure followed by a linear increase in the later stage and of the v(t) curve reaching a peak followed by a decrease toward a stabilized erosion rate v_s suggests that the surface undergoes mechanical hardening due to cyclic loading from shock waves and microjets generated by the implosion of cavitation bubbles;

- the sponge-like appearance of the eroded surface, with large cavities both in area and depth, indicates that the microstructure consists of coarse grains, whether of the base metal or of brittle intermetallic compounds;

- the variations in cavitation resistance parameters, as shown in the comparative histograms, generally indicate that artificial aging heat treatments and WIG remelting can induce beneficial structural changes in the surface of this alloy, making it suitable for use in parts exposed to moderate cavitation hydrodynamics;

- the values of the statistical parameters, such as the standard deviation and the accuracy of fitting the experimental data, confirm both the reliability of the artificial aging regimes and the rigor of the experimental procedure.

- he application of artificial aging heat treatments, especially at 140°C (regardless of the holding time), also leads to a reduction in the cavitation-affected surface area compared to that of the untreated (reference) alloy surface, from 74% down to 54%, which may serve as an additional parameter for assessing the cavitation phenomenon;

- artificial aging treatments also result in significantly reduced maximum cavitation penetration depths—more than two times lower—specifically 215 μm (for specimens aged at 140°C/24 hours), compared to 493 μm for the reference specimen;

- depending on the heat treatment regime, the increase in cavitation resistance of the aluminum alloy 6082 in the T651 condition ranges from 13% up to more than fourfold. The research results point to the heat treatment regime at 140°C, regardless of the holding duration (1 hour, 12 hours, or 24 hours), as the most favorable;

- the improvement of cavitation resistance of the 6082 alloy through WIG remelting proves to be a viable solution, but further research is needed on other processing parameters in order to significantly increase resistance, so the method could be applied to components such as ship propellers or hydraulic machine rotors (pumps) operating under intense cavitation erosion conditions.

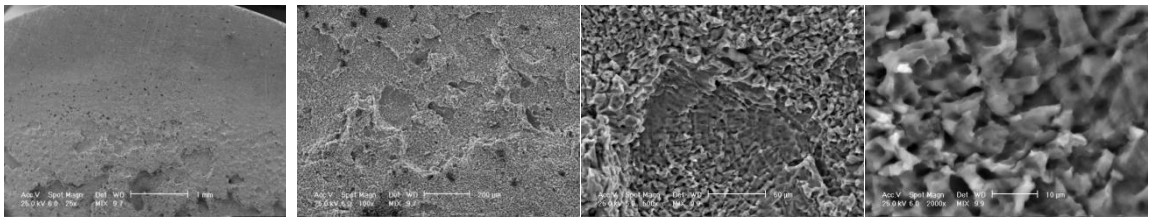
CHAPTER 6 – FRACTOGRAPHIC ANALYSIS OF SPECIMENS SUBJECTED TO CAVITATION FROM THE EXPERIMENTAL ALUMINUM ALLOY 6082 IN DIFFERENT STRUCTURAL CONDITIONS

This chapter presents the results of the fractographic analysis performed using scanning electron microscopy (SEM), at various magnification levels and for different structural conditions of the 6082 aluminum alloy, in order to identify the characteristics of fracture propagation caused by cavitation erosion. Ultimately, an attempt was made to establish a correlation between the material's condition and the fracture mode due to cavitation erosion. The analyzed samples were selected from specimens subjected to cavitation for a duration of 165 minutes, corresponding to artificial aging heat treatments at 190°C, 160°C, and 140°C, with a holding time of 24 hours at each temperature. The results were then compared with the fractographic features of the reference specimen in the T651 delivery condition, without heat treatment. Additionally, the entire fractographic study was compared to the results obtained by research teams from the Politehnica University of Timișoara and UNST, who conducted investigations on specimens from other aluminum alloys, specifically from the 5xxx and 7xxx series.

The fractographic features corresponding to the reference specimen, specifically the sample in the T651 condition (not subjected to artificial aging heat treatment), are shown in **Figures 6.1** and **6.2**. At low magnification (**Figure 6.1.a**), the presence of large open cavities ranging from 1 to 3 mm in diameter can be observed in the central area of the specimen, where cavitation damage is most severe. Toward the edges of the specimen, the surface appears finely roughened. At 100× magnification (**Figure 6.1.b**), the cavitation pits exhibit geometric shapes with sharp-edged boundaries, indicating material detachment due to dynamic tearing. At 500× magnification (**Figure 6.1.c**), sharp ridges within the cavities are observed, arranged in rosette-like formations, along with cleavage fracture propagation fronts. At 2000× magnification (**Figure 6.1.d**), the cavities appear angular with numerous intergranular cracks and the presence of (geometric, white-colored) compounds at the ridge tips. The quantitative and qualitative analysis of the cavitation-eroded surfaces of the reference specimen, as shown in **Figure 6.2**, highlights a cleavage-type fracture, associated with brittle compounds of the α-AlFeSi type.

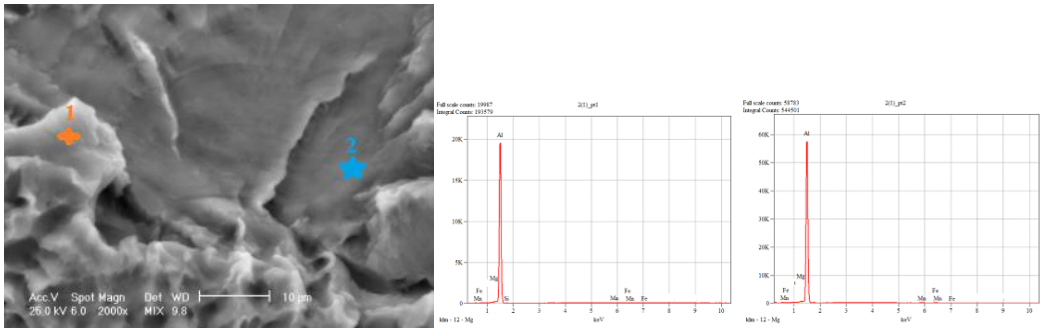
Analyzing the behavior of the 6082 alloy in its various heat-treated conditions, compared either with the 5083 alloy or the 7075 alloy, the following observations can be made: the surface features subjected to cavitation can be considered similar, displaying faceted cavities and a stepwise cleavage fracture propagation front, as aluminum alloys are generally part of the category of metallic materials with relatively low cavitation resistance. In the case of the 5083 alloy, where no

secondary phases exist to induce volumetric hardening with enhanced mechanical properties (e.g., martensite), cavitation erosion degradation is caused by the precipitation of secondary phases (Mg_5Al_8), which leads to the detachment of particles, leaving behind an eroded surface with numerous secondary cracks. In contrast, the 7075 alloy presents particularly large, angular cavities, generated by hardening compounds based on (Mg, Mn, Cu). These cavities are coalescent and interconnected, resulting in an extremely rough surface following cavitation erosion degradation.



a **b** **c** **d**

Figură 6.1 - SEM Images of the 6082 Aluminum Alloy Specimen, T651 Condition, Reference Sample, Subjected to Cavitation for 165 Minutes, at Different Microscope Magnifications: a - x25; b - x100; c - x1000; d - x500;



a **b** **c**

zona	*Microcompozitie chimică locală, %gr.*				
	Mg	*Al*	*Si*	*Mn*	*Fe*
1	0.43	98.43	0.00	0.71	0.20
2	0.60	97.84	0.54	0.43	0.43

d

Fig. 6.2 - SEM analysis of the aluminum alloy specimen in T651 condition, reference sample, subjected to cavitation for 165 minutes: a - SEM image; b - EDX at point 1; c - EDX at point 2; d - local microcomposition of the areas indicated in image a

CHAPTER 7 – CONCLUSIONS, ORIGINAL CONTRIBUTIONS, AND FUTURE RESEARCH DIRECTIONS AND PERSPECTIVES

7.2 ORIGINAL CONTRIBUTIONS

- Development of a literature synthesis on the physical metallurgy of precipitation phenomena in 6xxx series aluminum alloys, with a particular focus on alloy 6082, as an integral part of this series;
- Implementation of a complex experimental program involving the selection of experimental specimens made of 6082 aluminum alloy, the application of heat treatments selected based on in-depth documentation specifically artificial aging at 190°C, 160°C, and 140°C, each maintained for 1 hour, 12 hours, and 24 hours and the use of the most appropriate research methods and equipment to ensure the achievement of the initially proposed objectives;
- Complete structural evaluation of the experimental 6082 aluminum alloy specimens in different structural states, using optical metallographic microscopy, stereomicroscopy, scanning electron microscopy (SEM), and X-ray diffraction (XRD) analysis;
- Mechanical behavior assessment of the experimental specimens, by determining the main mechanical properties: tensile strength (Rm), 0.2% yield strength (Rp0.2), elongation (Z), Brinell hardness (HBW), Vickers microhardness (mHV), and impact toughness (KCV);
- Fractographic analysis of the fracture surfaces of Charpy KCV impact specimens at the macroscopic level using a stereomicroscope, aiming to identify the main structural features of dynamic impact fracture;
- Evaluation of cavitation erosion behavior of specimens in various structural states by constructing cavitation penetration depth and material loss rate curves, and performing a comparative analysis of cavitation resistance in order to identify the most suitable heat treatment that can enhance cavitation erosion resistance;
- Original assessment of the surface condition of specimens tested under cavitation erosion, through comprehensive fractographic analysis involving simultaneous examination using stereomicroscopy, optical metallographic microscopy, and scanning electron microscopy (SEM).

LIST OF PAPERS

ISI web of knowledge

1. Istrate, D; Sbarcea, BG; Demian, AM; Buzatu, AD; Salcianu, L; Bordeasu, I; Micu, LM; Ghera, C; Florea, B; **Ghiban, B. ,***CORRELATION BETWEEN MECHANICAL PROPERTIES-STRUCTURAL CHARACTERISTICS AND CAVITATION RESISTANCE OF CAST ALUMINUM ALLOY TYPE 5083*, Crystals, vol. 12, issue 11, 1538, doi: 10.3390/cryst121111538, published 2022
2. Ghera, C; Odagiu, OP; Nagy, V; Micu, LM; Luca, AN; Bordeasu, I; Demian, MA; Buzatu, AD; **Ghiban, B. ,***INFLUENCE OF AGEING TIME ON CAVITATION RESISTANCE OF 6082 ALUMINUM ALLOY*, University Politehnica of Bucharest Scientific Bulletin Series B-

Chemistry and Materials Science, Volume84, Issue4, Page225-237, Published 2022, Indexed2023-01-06

3. Ilare BORDEASU, Brandusa GHIBAN, Vasile NAGY, Vlad PARAIANU, Cristian GHERA, Dionisie ISTRATE, **Alin Mihai DEMIAN**, Petrisor - Ovidiu ODAGIU - Cavitational erosion resistance considerations for alloy 6082 state T651 - U.P.B. Sci. Bull., Series B, Vol. 85, Iss. 1, 2023, ISSN 1454-2331, Page 213-224,
4. Bordeasu, I; **Ghiban, B**; Micu, LM; Luca, AN; Demian, AM; Istrate, D, *THE INFLUENCE OF HEAT AGING TREATMENTS ON THE CAVITATION EROSION BEHAVIOR OF A TYPE 6082 ALUMINUM ALLOY*, Materials, Volume 16 Issue17, DOI10.3390/ma16175875, 2023
5. **Ghiban, B.,** Demian, A.M., Ghera, C. ,*CAVITATION BEHAVIOR STUDY OF THE AGING HEAT TREATED ALUMINUM ALLOY 7075*, Luca, A.N., Bordeasu, I., Journal of Physics: Conference Series, 2023, 2540(1), 012037
6. Bordeasu I, Ghiban B, Ghera C, Salcianu C. L , Micu L. M, Stroita D.C, *, Demian A.M, Buzatu A.D, *THE EFFECT OF HARDENING OBTAINED AFTER TIG REMELTING ON THE RESISTANCE OF THE 7075 ALLOY STRUCTURE TO CAVITATION EROSION,* U.P.B. Sci. Bull., Series B, Vol. 87, Iss. 1, 2025 ISSN 1454-2331, Page 163-178

BDI index papers

1. Dionisie ISTRATE, Claudia Lazar (Natra), Ovidiu Petrisor Odagiu, **Alin Mihai Demian**, Andreea Daniela Buzatu, Brandusa Ghiban - Influence of homogenization and aging parameters applied to mechanical and structural characteristics of alloy 5083, IOP Conference Series, Materials Science and Engineering, vol. 1262, 2022, open access, 012021, DOI 10.1088/1757-899X/1262/1/012021
2. Claudia Lazar (Natra), Dionisie ISTRATE, Ovidiu Petrisor Odagiu, **Alin Mihai Demian,** Andreea Daniela Buzatu, Brandusa Ghiban- Evaluation of mechanical characteristics of 3003 aluminum alloy plated sheets, IOP Conference Series, Materials Science and Engineering, vol. 1262, 2022, open access, 012021, DOI 10.1088/1757-899X/1262/1/012021

Conference proceeding papers

[1] Dionisie ISTRATE, Claudia Lazar (Natra), Ovidiu Petrisor Odagiu, **Alin Mihai Demian**, Andreea Daniela Buzatu, Brandusa Ghiban - Influence of homogenization and aging parameters applied to mechanical and structural characteristics of alloy 5083, ACME-02-01: Materials and Surface Engineering, June 9th, 2022, ACME , Iași, code, 2-015

[2] Claudia Lazar (Natra), Dionisie ISTRATE, Ovidiu Petrisor Odagiu, **Alin Mihai Demian**, Andreea Daniela Buzatu, Brandusa Ghiban- Evaluation of mechanical characteristics of 3003 aluminum alloy plated sheets, ACME-02-01: Materials and Surface Engineering, June 9th, 2022, ACME, Iași, code, 2-016

[3] Dionisie ISTRATE, **Alin Mihai DEMIAN**, Andreea Daniela BUZATU, Petrisor- Ovidiu ODAGIU, Brânduța GHIBAN -The influence of heat treatments on the mechanical and

structural characteristics of plastically deformed type 5083 aluminum alloys - 9th International Conference on Materials Science and Technologies – RoMAT 2022 November 24-25, 2022, Bucharest, Romania

[4] A. D. Buzatu, D. ISTRATE, **A. M. Demian**, Petrișor - Ovidiu Odagiu, B. Ghiban - Heat treatments influence on the mechanical behavior and structural characteristics of aluminum alloys type 2017 - 9th International Conference on Materials Science and Technologies – RoMAT 2022 November 24-25, 2022, Bucharest, Romania

[5] Petrișor- Ovidiu ODAGIU, D. ISTRATE, **A. M. Demian**, A. D. Buzatu, B. Ghiban-The influence of thermal treatments on the mechanical and structural characteristics of aluminum alloys type 6082- 9th International Conference on Materials Science and Technologies – RoMAT 2022 November 24-25, 2022, Bucharest, Romania

[6] **A. M. Demian**, A. D. Buzatu, Petrișor- Ovidiu ODAGIU, D. ISTRATE, B. Ghiban - Heat treatments influence on the mechanical and structural characteristics of 7075 aluminum type alloys- 9th International Conference on Materials Science and Technologies –RoMAT 2022 November 24-25, 2022, Bucharest, Romania